REPORT DOCUMENTATION PAGE	Form Approved OMB No. 0704-0188

1. REPORT DATE *(DD-MM-YYYY)*	2. REPORT TYPE	3. DATES COVERED *(From - To)*
01-07-2010	Journal Article	

4. TITLE AND SUBTITLE

Physical Pore Properties and Grain Interactions of SAX04 Sands

5a. CONTRACT NUMBER

5b. GRANT NUMBER

5c. PROGRAM ELEMENT NUMBER

6. AUTHOR(S)

Allen H. Reed, Karsten E. Thompson, Kevin B. Briggs, and Clinton S. Willson

5d. PROJECT NUMBER

5e. TASK NUMBER

5f. WORK UNIT NUMBER

74-7632-07

7. PERFORMING ORGANIZATION NAME(S) AND ADDRESS(ES)

Naval Research Laboratory
Marine Geoacoustics Division
Stennis Space Center, MS 39529

8. PERFORMING ORGANIZATION REPORT NUMBER

NRL/JA/7430-08-1

9. SPONSORING/MONITORING AGENCY NAME(S) AND ADDRESS(ES)

Office of Naval Research
800 North Quincy Street
Arlington VA 22217-5000

10. SPONSOR/MONITOR'S ACRONYM(S)

ONR

11. SPONSOR/MONITOR'S REPORT NUMBER(S)

12. DISTRIBUTION/AVAILABILITY STATEMENT

Approved for public release; distribution is unlimited

13. SUPPLEMENTARY NOTES

IEEE Journal of Oceanic Engineering, Vol. 35, No. 3

Abstract—**During the 2004 Sediment Acoustic eXperiment (SAX04), values of sediment pore properties in a littoral sand deposit were determined from diver-collected cores using traditional methods and image analysis on X-ray microfocus computed tomography (XMCT) images. Geoacoustically relevant pore-space properties of sediment porosity, permeability, and tortuosity were evaluated at scales ranging from the pore scale to the core scale from "mud-free" sediments collected within the 0.07-km^2 study area. Porosity was determined from water-weight-loss measurements to range from 0.367 to 0.369, from 2-D image analysis to range from 0.392 to 0.436 and from 3-D image analysis to range from 0.386 to 0.427. The range of permeability from all measurements was 2.8×10^{-11} m^2 to 19.0×10^{-11} m^2, however the range of permeability within each technique was much narrower. Permeability was determined using a constant head (CH) apparatus ($k_{range} = 2.88$ to 3.74×10^{-11} m^2), from a variant of the Kozeny–Carman (KC) equation ($k_{range} = 12.4$ to 19.0×10^{-11} m^2), from an effective medium theory technique ($k_{range} = 5.60$ to 13.3×10^{-11} m^2) and from a network model ($k_{range} = 8.49$ to 19.0×10^{-11} m^2). Permeability was determined to be slightly higher in the horizontal than in the vertical direction from the net-**

15. SUBJECT TERMS

Computed tomography, grain contacts, permeability, porosity, tortuosity

16. SECURITY CLASSIFICATION OF:			17. LIMITATION OF ABSTRACT	18. NUMBER OF PAGES	19a. NAME OF RESPONSIBLE PERSON
a. REPORT	b. ABSTRACT	c. THIS PAGE			Allen Reed
Unclassified	Unclassified	Unclassified	UU	14	19b. TELEPHONE NUMBER *(Include area code)* 228-688-5473

Physical Pore Properties and Grain Interactions of SAX04 Sands

Allen H. Reed, Karsten E. Thompson, Kevin B. Briggs, and Clinton S. Willson

Abstract—**During the 2004 Sediment Acoustic eXperiment (SAX04), values of sediment pore properties in a littoral sand deposit were determined from diver-collected cores using traditional methods and image analysis on X-ray microfocus computed tomography (XMCT) images. Geoacoustically relevant pore-space properties of sediment porosity, permeability, and tortuosity were evaluated at scales ranging from the pore scale to the core scale from "mud-free" sediments collected within the 0.07-km^2 study area. Porosity was determined from water-weight-loss measurements to range from 0.367 to 0.369, from 2-D image analysis to range from 0.392 to 0.436 and from 3-D image analysis to range from 0.386 to 0.427. The range of permeability from all measurements was 2.8×10^{-11} m^2 to 19.0×10^{-11} m^2, however the range of permeability within each technique was much narrower. Permeability was determined using a constant head (CH) apparatus (k_{range} = 2.88 to 3.74 $\times10^{-11}$ m^2), from a variant of the Kozeny–Carman (KC) equation (k_{range} = 12.4 to 19.0×10^{-11} m^2), from an effective medium theory technique (k_{range} = 5.60 to 13.3×10^{-11} m^2) and from a network model (k_{range} = 8.49 to 19.0×10^{-11} m^2). Permeability was determined to be slightly higher in the horizontal than in the vertical direction from the network model. Tortuosity ranged from 1.33 to 1.34. Based upon the small coefficients of variation for the conventionally determined pore-space properties, the sand sediment within these core samples was deemed homogeneous at all of the SAX04 sites. Additionally, grain interactions, specifically grain coordination number and grain contact areas, were determined from XMCT images. Grain contacts ranged in size from small point contacts of 136 μm^2 to large-area contacts the size of grain faces (>4500 μm^2). The mean coordination number was similar to that of a cubic packing (six), but sometimes exceeded 12, which is the coordination number for a hexagonal close packing of spheres.**

Index Terms—**Computed tomography, grain contacts, permeability, porosity, tortuosity.**

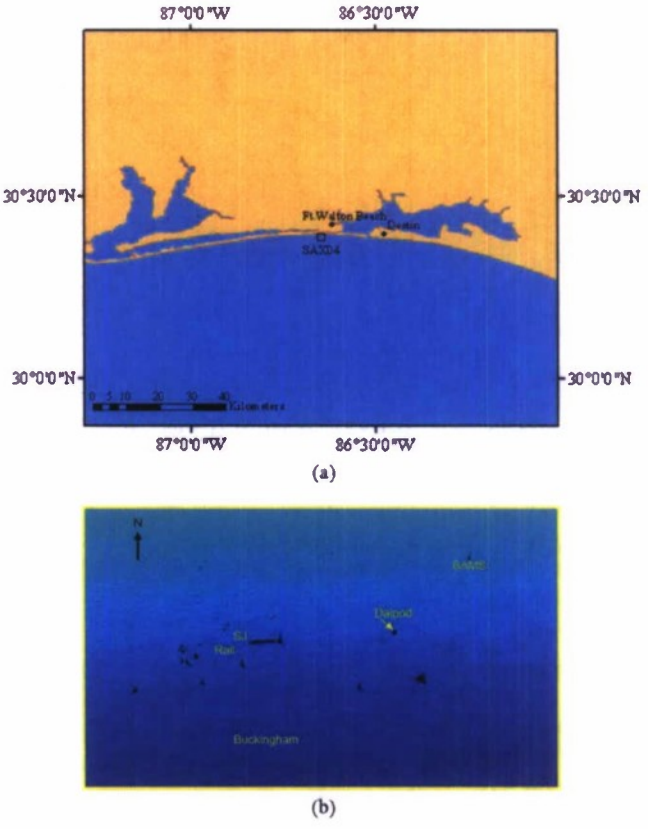

Fig. 1. (a) Study location located south of Fort Walton Beach and Destin, FL in the Northern Gulf of Mexico with the SAX04 study site bounded by the box. (b) The SAX04 study area located in approximately 17 m of water and the site locations are indicated on multibeam bathymetry imagery. Multibeam image courtesy of Kraft and de Moustier [5]. The following abbreviations demark sites where diver core samples were collected. SJ is the area where the *R/V Seward Johnson* was anchored. The Rail site is an APL-UW site that was ~50 m seaward of the *R/V Seward Johnson*. BAMS is the Benthic Acoustic Measuring System, which was positioned ~240 m to the east of the *R/V Seward Johnson*. Dalpod is the location of the Dalhousie Tripod, and Buckingham is the location of Mike Buckingham's array.

I. Introduction

ACOUSTIC propagation within, penetration into, and scattering from coarse-grained sediments displays a frequency-dependent response that is attributed to variability in sediment physical properties and may be attributed to fluid or grain motion during insonification [1]–[3]. This response suggests that properties of unconsolidated sediments affect acoustic behavior differently as the wavelength of the characteristic frequency changes [1], [2]. To address these issues, the 2004 Sediment Acoustic eXperiment (SAX04) was conducted. The primary goal of SAX04 was to address "high-frequency sound penetration into, propagation within, and scattering from the shallow-water seafloor" [4] by making acoustic measurements over a wide range of frequencies (i.e., 0.6–400 kHz). The measured results are compared to predictions from acoustic models, which were parameterized with properties of

Manuscript received June 04, 2008; revised July 22, 2009; accepted November 12, 2009. Date of publication April 26, 2010; date of current version September 01, 2010. This work was supported by the U.S. Office of Naval Research (ONR) Acoustics and the U.S. Naval Research Laboratory (NRL) Marine Geosciences Division, Program Element 0601153N. The NRL contribution number is JA/7430-08-00014.

Associate Editor: J. F. Lynch.

A. H. Reed and K. B. Briggs are with Seafloor Sciences Branch, Naval Space Center, MS 39529 USA (e-mail: allen.reed@nrlssc.navy.mil).

K. E. Thompson is with the Cain Department of Chemical Engineering, Louisiana State University, Baton Rouge, LA 70803 USA.

C. S. Willson is with the Civil and Environmental Engineering Department, Louisiana State University, Baton Rouge, LA 70803 USA.

Color versions of one or more of the figures in this paper are available online at http://ieeexplore.ieee.org.

Digital Object Identifier 10.1109/JOE.2010.2040656

unconsolidated, subaqueous, sandy sediments collected from the study area (Fig. 1), and which are presented elsewhere in this JOURNAL.

The models that predict acoustic properties in sand frequently assume that the sediment frame is rigid and immobile [1], [6], [7]. Recently, motion, compression, and dilation of the sediment frame have been invoked to account for sound-speed dispersion and acoustic attenuation, which are not accurately predicted by the Biot and Biot-based models in the high-frequency domain [1]–[3], [8]. Therefore, further evaluation of the issues associated with grain motion and changes in the frame modulus during insonification, such as frictional resistance to loading, are required to understand the loss mechanisms during insonification.

The broad success of the Biot model is evident in its ability to predict sound speed in the limits of 20–400-kHz range and attenuation measurements in the limits of 20–100-kHz range [4], [6], [9]. However, model predictions of sound speed and attenuation, during the 1999 Sediment Acoustic eXperiment (SAX99), exhibited large discrepancies with measured values over a wide range of acoustic frequencies [1]. The principle cause for this discrepancy was attributed to four Biot-parameters: porosity, tortuosity, permeability, and grain modulus. To address the importance of specific Biot parameters, the effective density fluid model (EDFM) was created. Results from the EDFM were comparable to those obtained by the full Biot model, and they demonstrated that the properties of the granular frame could be treated as relatively unimportant, *per se*, by eliminating the bulk and shear modulus of the frame [10], [11]. However, as with the Biot model, the EDFM is unable to account for the discrepancies between modeled and measured results for sound speed and attenuation at higher frequencies.

To address the mismatches between model and measured acoustic attenuation in sands at high frequencies (>100 kHz), several models invoke and incorporate grain motion, specifically, translation and shearing at grain contacts, which would result in a dynamic frame moduli [2], [3], [8], [12]. The intergranular friction between grains and the potential for slippage at the contacts require evaluation, yet isolating and evaluating grain contacts, which exist at submicrometer to micrometer scales, has only been addressed in a limited number of cases.

There are numerous approaches to quantify porosity, permeability, and tortuosity. One approach is to combine 2-D or 3-D image acquisition with image analysis. In this approach, high-resolution images of complex granular media are collected that accurately resolve sand grains and the surrounding pore space. Then, image analysis is used to quantify grain and pore properties. As imaging and image analysis capabilities have improved, sediment bulk properties are more easily and accurately derived from pore space and grain characteristics within granular media, such as the sands at the SAX04 site. For example, porosity is classically determined from the ratio of water content to sediment volume. With image analysis techniques, porosity is determined as the ratio of pore area to sediment area (2-D) or pore volume to bulk sediment volume (3-D) after the grain and pore space are differentiated from images that have resolutions greater than 10 m [13]–[15].

Permeability is typically calculated from Darcy's Law from direct measurements of fluid discharge, the pressure gradient, fluid density, and fluid viscosity [16]. Permeability can also be empirically determined from porosity, grain size, and particle shape using the Kozeny–Carman (KC) equation, which is based upon a hydraulic radius or conduit-flow model [17]. More recently, image-based determinations of pore-size distributions are accounted for using a network of conduits of various sizes [18], [19]. In this approach, pore bodies (nodes in the network) are distributed in a network and linked by pore throats (conduits or pipes for flow). Pore bodies serve as flow junctions and account for void volume in these models, while pore throats serve as conduits between the pore bodies and provide frictional resistance to flow. This idealized breakdown of the pore space is illustrated using a cross section of a real material in Fig. 2. Permeability determinations from network models that operate on volumetric images have a distinct advantage over conventionally made determinations, because fluid flow can be determined in multiple directions on the same sample. This ability makes it possible to verify sediment isotropy, an assumption that is inherent to 2-D image analysis and to the Biot model.

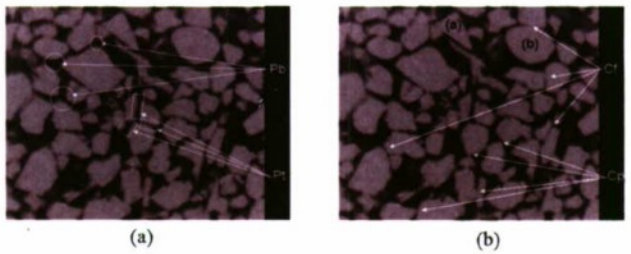

Fig. 2. An X-ray microfocus computed tomography "slice," or 2-D image, used for quantification of pore space and prediction of permeability with the effective medium theory method [14]. (a) Pore throats (Pt), or the elongated features between grains, and pore bodies (Pb), the connection points between the grains. (b) Depicted grains are angular or well rounded and the contacts between the grains vary from large-areal face contacts (Cf) to small-area contacts, or point contacts (Cp). Images are 2.65 mm along the base.

Tortuosity has been determined here, solely using image analysis. It is related to the path length through the ramified pore space around the grains, such that it may be altered as density of grain packing increases and as the pore sizes decrease. It is an evaluation of the fluid flow path through the sample and around the grains that deviates from a straight-line path across the sample. As such, it is often added to fluid-flow equations in sediments which have fluid paths that deviate from that of a straight pipe. Consequently, it has proved to be an important correction to Poiseuille flow through a straight pipe as noted in the sinuosity term (tortuosity to the half power) inherent in the Biot model [17]. It is commonly incorporated in acoustic models as the sinuous path, the flow path, through the sediment divided by the straight-line distance through the sediment squared, as was the case during SAX99 [20]. As its value may vary directionally through sediment strata or due to different packing regimes or grain orientations, differences in the value of tortuosity through different planes may be used to indicate sediment isotropy or anisotropy [16]. This is based upon the idea that longer path lengths typically yield lower flow rates and permeabilities, provided the pore radii remain the same size or become smaller. For instance, in highly ordered and idealized packing of monosized, spherical beads, a constant value of 2 was assumed in all

directions [17], yet in thin platy materials with high aspect ratios tortuosity may be much higher through the vertical than through the horizontal plane of the sediment bed. Cubic or hexagonal close packing of spheres is atypical in natural geologic materials, which have pore-scale heterogeneity due to grain size distribution, variability in grain aspect ratio, and complex shapes. The complexity of the resulting pore space and its influence on flow properties can be addressed and quantified using a network, similar to an electrical circuit, of interconnected pore bodies (junctions) and pore throats (conductors) of varied sizes [14], [21].

In addition to direct evaluation of the pore space and quantification of relevant geoacoustic properties, direct evaluation of the grains and quantification of grain properties is also possible from X-ray microfocus computed tomography (XMCT) images. The challenge is to quantify properties of the grains and the interactions between the grains from these images. The complexity of grain shapes makes quantifying grain properties a challenge because grain shapes, surface morphology, and contacts between grains are geometrically irregular. Surface morphological features, specifically surface roughness that determine coefficients of friction may be impossible to resolve with XMCT, due to resolution limits, but may be resolved with scanning electron microscopy (SEM). Potentially, surface roughness may be resolved more effectively with higher resolution scanners, such as nanometer-resolution CTs or neutron tomographs. Due to resolution limitations associated with XMCT and the mathematical complexity of addressing highly irregular grain shapes and grain contacts, grains are typically modeled as discrete particles with relatively simple particulate geometries that have uniform shapes, predictable grain contacts, and finite degrees of freedom. The surfaces of these simple grains are typically smooth, linear, and/or curvylinear with no concavities. Spheres are a good example as they are commonly used as an analog to an assemblage of sand grains; they have a readily discernible and well-understood shape, and a simple and singular contact type (a point contact) [22]. More complex than spheres, the square-ended cylinder serves as another useful grain analog. It has flat, linear, and curvylinear surfaces, such that there is more variability in grain orientations, packing density, and contact types, which may occur as point, edge, or face contacts [23], [24]. Spheroids and ellipsoids, as well as cylinders and spheres, have proven useful in pore-scale evaluations of sediment physical properties, because they enable theoretical limits of geoacoustic properties to be determined as a function of particle nonsphericity and packing density [25]. Additionally, these shapes provide a great deal of insight into controls of physical properties of sand sediments, such as porosity, permeability, tortuosity, and grain interactions, as packing density increases from a minimum to a maximum density [23]–[25].

To evaluate grain–grain interactions, it is necessary to isolate individual grains within the 3-D images of the grain assemblage. This is far easier when the grain geometry is well known than it is for irregularly shaped sand grains. Previously, grain contacts and interactions have been determined from scattered grains on a microscope stage or 2-D images of samples in cross section (e.g., thin sections or SEM polished "stubs"). This is problematic in that 2-D images provide insufficient realizations and dimensionality of contacts to adequately address the types and areas of the contacts [13], [14]. Confocal microscopy is able to yield a great deal more information about grain interactions with detailed pictures of 3-D grain and pore structure [25], [26]. However, XMCT appears to display the best capability to obtain larger volumes, appropriate for obtaining average pore structure, determining flow properties, and quantifying grain parameters [27]. Recent advances have been made to quantify geometrical properties of natural sand grains from 3-D images (XMCT) using algorithms that discretize the grains within a 3-D assemblage. The grain properties (e.g., size, volume, aspect ratio) can then be quantified for the individual grains and the contacts between grains can be addressed (see [23] for more details).

Here, our objectives are to quantify several geoacoustic parameters: porosity, permeability, and tortuosity, using a variety of methods that evaluate these properties at core scales to grain scales to pore scales and to assess the homogeneity of surficial samples collected throughout the SAX04 site. Pore properties were determined from sand cores collected from several locations throughout the SAX04 field by using traditional measurements and/or image analysis to provide geoacoustic parameters at a range of spatial scales for what is typically a sand body devoid of mud (Fig. 1). We compare values of permeability determined from direct measurements with permeability determinations made from the KC equation, effective medium theory (EMT) modeling evaluations of pore space in 2-D images, and 3-D network modeling that operates within the confines of the 3-D pore structure extracted from XCMT images [14], [28], [29]. Note that it is our opinion that each set of determinations should be evaluated based upon the potential limitations inherent to the specific technique, that is, one technique should not be deemed superior to another as each method has unique advantages. Additionally, we evaluate the types of grain contacts present and quantify the number and areal extent of these grain contacts. In doing so, we have addressed several of the critical parameters required to extend acoustic modeling to higher frequencies, that is, frequencies greater than 100 kHz [1]. These volumetric images also provide the basis for the grain analyses, which includes the number, areal extent, and types of grain contacts. The range of grain contacts encountered in these images should assist acoustic modelers to further develop theories and models on the role that granular motion may play in attenuation and sound-speed dispersion at high frequencies.

II. Study Site

The SAX04 study site was located south of Fort Walton Beach, FL, in the northern Gulf of Mexico, on the Mississippi–Alabama–Florida (MAFLA) sand sheet, in ~17 m of water. The experiments were conducted within a relatively small, 460 × 360 m^2, area that was surrounded by a large body of relict quartz sand with up to 98% sand-sized particles [30]. This area had previously been determined a homogeneous deposit of relict siliciclastic (quartz) sand with trace amounts of mafic minerals and minute amounts of clay minerals (Fig. 1) [14], [30]–[33].

After chirp data were collected in May 2004 and the area was determined to be mostly "benign" and "relatively free of subsurface structure" [32], several storms altered the sediment

structure by introducing large quantities of mud into a sediment that was previously composed of well-sorted, medium-sized quartz sand. The storms that had an impact on the SAX04 study area during the 2004 Hurricane Season were Hurricanes Charley (August 9–14), Frances (August 25–Sepember 8), Ivan (September 2–24), and Jeanne (September 13–28) and Tropical Storms Bonnie (August 3–13) and Matthew (October 8–10). These storms suspended muddy sediments outside the experiment area before and after commencement of the SAX04. Suspended mud was transported into the experiment area, thereby altering the sandy sediment deposit and introducing wide scale heterogeneity into surficial sediments [34]. During the course of the SAX04, much of this mud was apparently transported out of the study site, yet some was incorporated into the sandy bed and retained as interbedded deposits [35]. The focus of this paper is to quantify pore properties and grain interactions in the areas that remained mud-free and characteristic of the typical MAFLA sand sheet [30], therefore cores containing mud are not addressed in this paper.

III. Methods

A. Core Sample Collection, Preparation, and Analysis

Sediment samples were hand-collected by scuba divers using thin-walled polycarbonate, 6.3-cm-outside-diameter cores from areas where surficial sediments were obviously sandy. Visual evaluation of the sand through the clear polycarbonate cores assisted in evaluation of the cores for mud [35]. Several such diver-collected cores were obtained at each of the SAX04 sites for conventional determinations of grain size, porosity, and permeability. Other diver-collected cores were obtained for X-ray microfocus computed tomography (XMCT) imaging; these cores were impregnated with resin and subcored to small-diameter (8 mm), representative elemental volumes, before scanning with the XMCT. A representative elemental volume contains ~6–10 grain diameters per plane and sufficient material to predict bulk geoacoustic properties.

1) Conventional Determinations From Cores: After the diver cores were returned to the ship, they were allowed to equilibrate with laboratory temperature and pressure before determinations of sound speed, sound-speed attenuation, bulk porosity, and permeability [35]. Grain size was determined by sieve analysis and porosity was determined by the water-weight-loss method and at 2-cm intervals from the diver-collected cores, which were transported to a shore-based laboratory before these analyses (see [35] for methodology).

Hydraulic conductivity was determined from constant-head permeameter (a modified Soiltest K-605 combination permeameter) measurements of volumetric fluid discharge during a measured time interval on 13-cm-long diver cores. Seawater was used to maintain a constant hydraulic head on the core sample. For each core, three to five consecutive, temperature-monitored measurements were made. Permeability (k), often called the permeability coefficient with units of length squared, was then determined from Darcy's law

$$k = \frac{A}{\mu Q}(\Delta P) \tag{1}$$

where Q is the volumetric flow rate for a fluid with dynamic viscosity μ driven through a core of area A by a pressure gradient ΔP, which is determined by the hydraulic head. Dynamic viscosity was estimated from the measured temperature and salinity of the seawater. Sound-speed and attenuation measurements were made using a 400-kHz transducer through the temperature equilibrated diver-collected cores [35].

2) Core Impregnation for XMCT: Diver-collected cores were "lithified" to enable subsampling and subsequent high-resolution (pore-scale) imaging using the XMCT system. The samples were lithified by impregnating the pore space with a low-viscosity, polyester casting resin. The resin displaces the water during vacuum-driven infiltration, cures without changing volume, and fixes grain coordinates and orientations during the curing process, as demonstrated during SAX99 [14], [36]. Once the entire core cured, 2-cm-thick disks were cut with a diamond blade from the solidified core, and 8-mm diameter subsamples were cut from the center of the disks with a diamond-tipped coring tube. These small-diameter subsamples allow high-resolution images of a representative elemental volume of sand to be produced with the XMCT. The XMCT image data are composed of 11.43-μm voxels (3-D pixels), which facilitates the analysis of sand grains and pore structure. Practically, this resolution provides ~31 voxels per grain (mean grain diameter: 363 μm). For the permeability analysis, the representative volume removed from the scanned core was 40.3 μm^3, to provide 9.44 times the mean grain size of 363 μm, which is a sufficient number of voxels (3-D pixels) per pore or grain diameter to be statistically representative [37].

B. Empirical Estimation of Permeability From Porosity and Grain Size

When permeameter measurements are unfeasible or unavailable, permeability is commonly predicted from sediment porosity and the specific surface area of the grains using the KC equation, which is a hydraulic radius model that assumes Poiseuille flow within individual, circular pipe-shape pores

$$k = \frac{d^2 n^3}{180(1-n)^2}. \tag{2}$$

In this equation, permeability is determined from the mean grain size d and the porosity n (commonly determined from the water-weight-loss method). This equation, and the numerical constant in the denominator, is applicable to unconsolidated sediments; it accounts for the grain specific surface area and tortuosity, or deviation from a straight-line path, through the sediment [38].

C. Pore Property Determinations From XMCT

The XMCT analysis generates 3-D volumetric data based on X-ray attenuation, which is affected by sample density and elemental composition. In this procedure, photons are produced and accelerated in an X-ray tube where they strike a tungsten target to produce X-rays. The X-rays are projected through an aperture and the sand sample towards the detector array, which is a charge-coupled device (CCD) at the base of a phosphor screen that effectively amplifies the intensity of the X-rays. The projection of the X-ray beam as a cone through the sample towards the

screen magnifies the sample attenuation, therefore high resolution is achieved on small samples that are placed close to the aperture of the X-ray tube. Because the X-ray attenuation data are recorded at thousands of projection angles while the sample rotates within the X-ray beam, an image with high clarity and well-defined pore-grain boundaries is produced. Once collected on the CCD array, attenuation data are converted to gray-scale values with a single value assigned to each voxel within the image. Voxels (3-D pixels) represent the X-ray attenuation of the sediment matrix at specific locations within the scanned sample. X-ray attenuation is a function of the material density and atomic number of the sample [39]. The attenuation values are converted to 16-b gray-scale values and then the spectrum of gray-scale values that comprises the images is converted to a 1-b image comprising pore space (voxels assigned 0s) and grains (voxels assigned 1s). This process is called segmentation which is performed with an indicator kriging algorithm [40], [41]. The XMCT image of the sediment is represented by a spectrum of gray-scale valued voxels with two characteristic peaks: one for the pore space and one for the grains. Two values are chosen to create the 1-b image. First, a value on the lower end of the spectrum and a value on the higher end of the spectrum are selected to separate the spectrum into three parts: one for pores, one for grains, and one for voxels that are not clearly part of the pore or grain population. Voxels at the lower end of the spectrum up to the selected value are assigned to the pore space and voxels at the highest end of the spectrum to the upper selected value are assigned to the grain space. This leaves the saddle or middle portion of the curve without an assignment, due to the uncertainty of whether theses voxels are part of the pore space or part of the sand grains. In these cases, the values of the neighboring voxels are used to make the assignments; if the majority of the neighboring voxels belong to pores, then the voxel is assigned to the pore population and to the grains otherwise. After the pores are assigned a value of zero and grains are assigned a value of one, porosity is easily determined as the ratio of 0-valued voxels divided by the total number of voxels in the image (note: in 2-D porosity determination, pixels are evaluated and the porosity is determined as the ratio of 0s to the total number of pixels in the image).

Permeability, as with the porosity, can also be determined from 2-D or 3-D images of the pore network structure. In these binary images, the pore space is bounded by grains, through which we assume that there is no fluid flow. To convert the pore space of a 3-D image into a pore network, the midpoints of all the pores are determined and formed into a medial axis. This is similar to the pore skeleton that is used in 2-D images; the midpoints of the pore space in the 2-D images are determined and joined together during a process called "skeletonization" [41]. The binary image is simplified into highly ramified paths by selecting voxels at the center of the pore space. The paths that comprise the medial axis are then broken into pore throats, or paths between intersections with other pore throats. These intersections are called the pore bodies. The pore throat dimensions, much like in a pipe, are the axial length of the path and the cross-sectional area of that path. The pore bodies are viewed as a circle with the radius of this circle being the dimension of the pore body that is relevant to fluid flow. The coordination number for each pore body is the sum of pore throats that intersect at that select pore body [Fig. 2(a)]. The pore space is surrounded by sand grains, which serve as impermeable boundaries for fluid flow [Fig. 2(b)]. By quantifying the sizes of the pores and the number of connections for the pores, specifically the pore throat dimensions and number of pore throats that intersect a pore body, permeability can then be determined using an effective medium approach [14], [28]. In the effective medium approach, the pore throat dimensions, the pore body radius, and the average coordination number within a given 2-D image are quantified using common image analysis routines. A skeletonization routine is used to determine the length (l_t) and average pore connectivity (z), while a Euclidean distance map is used to determine the pore throat radius (r). In this case, the images were removed from the horizontal plane of the XMCT image volumes. With EMT or any prediction of bulk sediment properties that originates from 2-D image data, sample homogeneity is assumed. Within each 2-D image, conductivity $(g(r_i))$ of each pore throat (1 to i, the total number of pore throats in the image) is determined from the radius and length of the discrete pore using the Poiseuille equation

$$g(r_i) = \frac{\pi r^4}{8 l_t}. \tag{3}$$

The average conductivity for the entire image, and hence the sample, is then solved iteratively for an effective pore throat radius (r^*) by

$$\sum_i n_t(r_i) = \frac{g(r^*) - g(r_i)}{g(r_i) + \left[\frac{z}{2} - 1\right] g(r^*)} \tag{4}$$

which assumes that a probability distribution function of pore throat radii $(n_t(r_i))$ has been determined in the form of a histogram where r_i denotes the pore throat at the ith radius interval. Once the effective pore throat radius r^* is determined for the image, it is possible to solve for the permeability (k) using

$$k = \frac{n}{8T} \frac{r^{*4}}{\langle r_{pc}^2 \rangle}. \tag{5}$$

In (5), sample porosity (n), average tortuosity (T), the effective pore radius (r^*), and the spatial average of the pore space through which the conduction is occurring $\langle r_{pc}^2 \rangle$ are accounted for. Further details and images used in this procedure have been presented previously in this journal and elsewhere [14], [28].

As with EMT, network modeling is an approximate technique that relies on evaluating the characteristic sizes and dimensions of the pores and pore throats, and modeling Poiseuille flow through a simplified structure. However, network modeling (especially image-based techniques) differs from EMT in an important way. That is, network modeling also accounts for spatial correlations and 3-D interconnectedness of the pores. Once the network model is constructed (and conductances are assigned to the pore throats), permeability can be calculated by simulating fluid flow and substituting the results into Darcy's law [19], [28].

Typically, pore throats and pore bodies are determined from a binary image by mapping the interconnected network and then assigning pore-throat conductances according to the sizes of flow paths [41]. In this work, the grains from the sediment

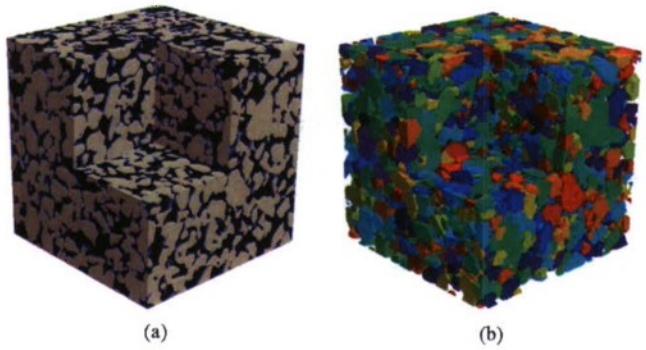

Fig. 3. Volumetric image of SAX04 sand from the *R/V Seward Johnson* (SJ) site that is typical of the XMCT images used in these analyses. (a) Pores are blue and grains are gray in the segmented image. (b) The grains are discretized. Colors are used to visualize the separate grains. Note: colored grains are used to differentiate one grain from a neighboring grain; colors do not indicate binning by size or other characteristics. Each edge dimension is 300 voxels or 3.43 mm.

samples are discretized first (Fig. 3) [23]. Once the grain structure is defined, a Delaunay tessellation is used to define possible pore locations [19], [42]. The Delaunay cells are used as seed points within the void space to locate maximal spheres, which are treated as pore centers. The connectivity of the pore space is then defined directly from the voxel image, and a series of geometric parameters are computed to complete the network description [29], [37].

Tortuosity is determined from the medial axis (or skeleton) of the binary images, and therefore, it is determined from the length of the path that follows the midline of the pores through the sediment. The actual flow path is assumed to be the midline of the pores, although this may be debated. To quantify pore path lengths, the pore-grain boundary is determined throughout the volume of sediment. Then, voxels are assigned incrementally higher values away from the pore-grain boundary and towards the central portion of the pore. Once all voxels are assigned a value, the highest valued voxels are joined to form the medial axis, or skeletal midline, of the pores [41]. Path lengths are determined from a medial axis image of the pore space. The length of the sinuous paths between the pore bodies on adjacent sides of the image, and therefore, through all dimensions of the image, are then determined. The straight-line distance between the centers of the pore bodies on the adjacent sides of the image is also determined. From these determinations, the ratio of the sinuous path length to the straight line path is determined. This is referred to as sinuosity by Biot [6]. Tortuosity, in keeping with current usage in geoacoustics, is calculated as the square of the sinuosity [1], [20].

D. Quantification of Grain-Contact Areas and Coordination Numbers From XMCT Images

Sand grains provide the framework in which porosity and tortuosity are determined, and through which fluid is transported. The importance of the granular framework on the development of porosity, permeability, and tortuosity and its relationship to bulk and shear moduli is widely addressed. However, the nature of grain interactions, that is, the area over which grains are in contact and the number of contacts that exist per grain

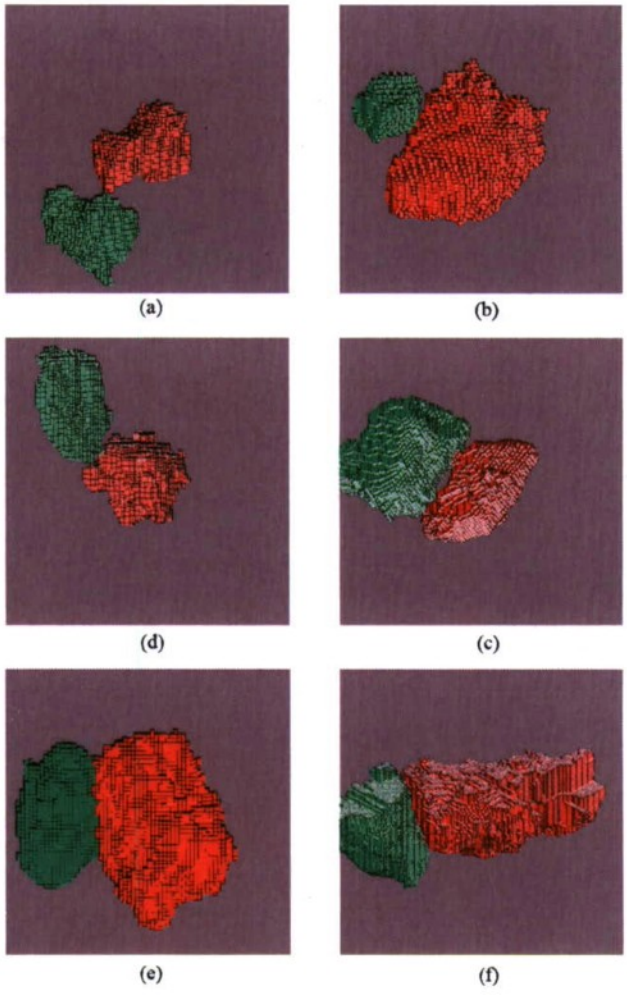

Fig. 4. Grain contacts cover varied areal extent. They also appear in many forms, from point contacts (a) and (b) to multiple point contacts or microasperities (c) and (d) to edge and face contacts (e) and (f). Dark lines correspond to the edges of voxel. The grain contacts in (e) and (f) are larger than those addressed in numerical models of grain interactions.

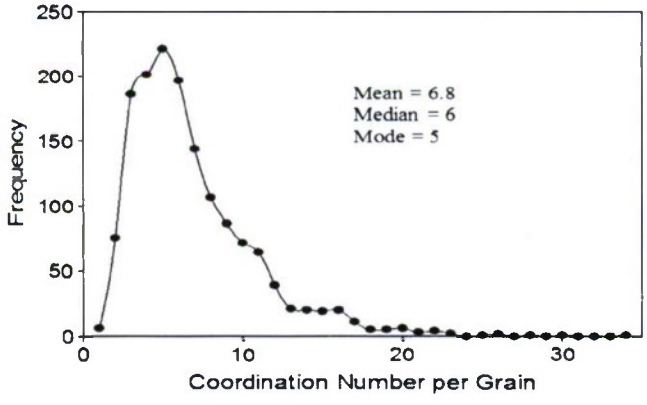

Fig. 5. Coordination number for SAX04 sediments is depicted in this cumulative frequency distribution. This wide range of coordination numbers varies from the fixed coordination number found in ideal packings.

(i.e., the coordination number) is rarely addressed and the influence of the contacts on friction angle and resistance to intergranular motion is poorly understood. To obtain information

TABLE I
AVERAGE VALUES OF POROSITY (WATER-WEIGHT-LOSS METHOD), PERMEABILITY (CONSTANT-HEAD METHOD: CH) DETERMINED FROM SURFICIAL SEDIMENT, AND PERMEABILITY PREDICTED FROM KOZENY–CARMAN (KC) EQUATION AND THE MEAN GRAIN SIZE FOR SAMPLES EVALUATED

Sample Site	Porosity	±1 s.d.	K $\times 10^{-11}$ (m^2) CH	±1 s.d. $\times 10^{-11}$	k $\times 10^{-10}$ (m^2) KC	Mean grain size (mm)
R/V Seward Johnson	0.369	0.007	2.88	0.053	1.24	0.351
Buckingham	0.367	0.004	3.09	0.765	1.90	0.392
Rail	0.368	0.006	3.74	0.551	1.49	0.330
Dalpod #1	0.368	0.004	3.03	0.502	1.28	0.366
BAMS	0.366	0.006	2.80	--	1.33	0.379
Mean	**0.368**		**3.11**		**1.448**	**0.364**

TABLE II
PHYSICAL PROPERTIES OF SURFICIAL SAMPLES (TOP 2 cm OF THE CORE) FROM 2-D IMAGE ANALYSIS AND EMT MODELING THROUGH THE VERTICAL PLANE FROM SEVERAL SAX04 SAMPLING LOCATIONS. IMAGE RESOLUTION 11.43 μm

Sample Site	Porosity	±1 s.d.	k $\times 10^{-11}$ (m^2)	±1 s.d.($\times 10^{-11}$)	No. of samples
R/V Seward Johnson	0.421	0.03	13.3	6.32	6
Buckingham	0.436	0.02	7.75	1.30	6
Rail	0.392	0.05	6.93	0.854	3
Dalpod #1	0.417	0.01	6.83	0.835	3
IMP	0.384	0.02	6.94	0.660	3
Mean, between sites	**0.410**		**8.35**		
Site Mean (all samples)	**0.411**	**0.0322**	**8.97**	**4.32**	

on sand grains and their associated contacts, XMCT images of the grain surfaces were evaluated and quantified using the algorithms described in [23]. Data from this analysis can be used to quantify grain properties (i.e., location, aspect ratio, surface area, volume) and isolate grain contacts for evaluation. The evaluations are based upon grain-contact types, such as point contacts (single voxel) or face contacts (multiple voxels) (Fig. 4) and coordination number or the number of contacts per grain (Fig. 5). At any one of these contacts, the surface area at the contact interface is quantified using an adaptation of an accurate surface-area algorithm, developed by Lindblad for know grain shapes (Fig. 5) [37], [43]. Therefore, XMCT images provide a basis to evaluate grain contacts in a granular assemblage, to address the deviation of coordination numbers from that found in idealized spherical packings, and to quantify the contact area from single points to large areas (Figs. 4–6).

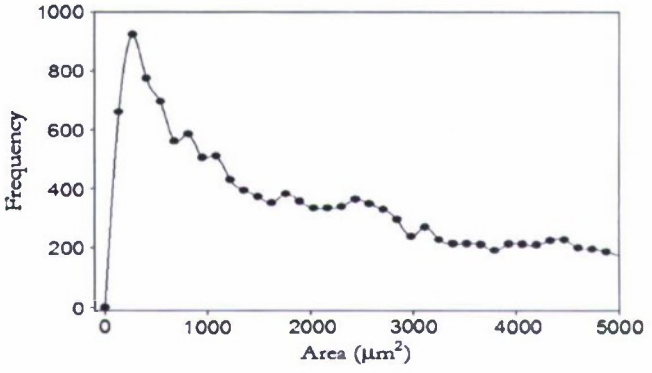

Fig. 6. Contact area for a SAX04 sediment sample is depicted in a cumulative frequency distribution. The contact areas from the SJ surficial sediment sample ranged from point contacts where one grain contacts another grain on one voxel surface (136 μm^2) to areal contacts comprising many adjoining voxels (37 voxels at 5012 μm^2).

IV. RESULTS

A. Porosity, Permeability, and Mean Grain Size From Traditional Methods

Sediment porosity was determined on 2-cm-thick sections of 5.9-cm-inside-diameter samples from diver-collected cores. The values of porosity in sand without obvious amounts of storm-derived mud display a very small degree of variability among the 11 locations within the SAX04 site (Table I; [35]). Permeability values determined from the constant-head (CH) permeameter on diver cores that were also mud-free show little variability within the SAX04 site (Table I). The sediment is a moderately well-sorted, medium sand with a mean grain size of 1.47ϕ (363 μm) and a coefficient of variation (CV) of 10.19 [35].

B. Kozeny–Carman Permeability Predictions

The mean grain size (d) and porosity of SAX04 sands at each site provide the basis for predicting permeability using the KC equation [see (2)], which yields permeability predictions of 5.0 to 6.3×10^{-11} m^2 (Table I).

TABLE III
AVERAGE BULK POROSITY FROM VOXEL COUNTING. PERMEABILITY [IN x, y (HORIZONTAL), AND z (VERTICAL) DIRECTIONS] AND TORTUOSITY PREDICTED FROM 3-D XMCT IMAGES WITH NETWORK MODELING. IMAGE RESOLUTION IS THE SAME AS FOR THE 2-D ANALYSIS (11.43 μm)

Sample Site	Depth (cmbsf)	Porosity	Permeability ($\times 10^{-10}$ m^2)			Tortuosity $(L_o/L_s)^2$
			x	y	z	
R/V Seward Johnson	0-2	0.411	1.25	1.30	0.97	1.34
	5-6	0.423	1.27	1.28	1.08	1.34
	9-10	0.414	1.36	1.31	1.08	1.34
Buckingham	0-2	0.419	1.28	1.25	1.01	1.33
	5-6	0.406	1.23	1.27	1.07	1.33
	9-10	0.394	1.40	1.30	1.04	1.33
Dalpod 1	0-2	0.427	1.56	1.58	1.41	1.33
	5-6	0.411	--	--	--	1.33
	9-10	0.414	1.90	1.73	1.43	1.34
IMP	0-2	0.397	1.41	1.39	1.18	1.34
	5-6	0.399	1.79	1.74	1.24	1.33
	9-10	0.414	1.11	1.09	0.85	1.33
Rail	0-2	0.397	1.17	1.06	0.99	1.33
	5-6	0.403	1.08	1.06	0.92	1.34
	9-10	0.386	--	--	--	1.33
Mean		**0.408**	**1.38**	**1.34**	**1.11**	**1.333**
±1 s.d.		0.012	0.25	0.23	0.18	0.004
Minimum		0.386	1.08	1.06	0.849	1.3261
Maximum		0.427	1.90	1.74	1.43	1.3406

C. Porosity and Permeability Determinations From 2-D Images

Sediment porosity and permeability predictions from 2-D images are generally in agreement with the determinations of these two sediment properties using traditional methods from entire cores, despite being estimated from images that represent a much smaller area of the sand volume. In this case, permeability was predicted from a 2-D image, which is a single horizontal slice removed from the XMCT volume (Tables I and II). Two-dimensional image data are derived from 9-mm^2 planar sections, whereas porosity determined from water weight loss is derived from 54.7-cm^3 samples and permeability determined using a constant head (CH) device is derived from 355-cm^3 samples. The 2-D image data display greater variability than the conventionally determined values [14], [15]. The values of permeability predicted from 2-D images using an EMT approach were usually twice, and up to three times, the CH values (Table I). It is important to note that predictions of porosity and permeability made from 2-D images of sediments only apply to the top centimeter section of the core samples that were analyzed, whereas the conventional determinations of porosity applies to the 0–2-cm interval and permeability applies to the top 13 cm of sediment. Due to the uniformity of bulk density and porosity values below the upper 10 centimeters below the seafloor (cmbsf) from 23 cores collected throughout the SAX04 site, we assumed that shallow sediments (up to 10 cmbsf) would display the greatest variability in physical property values. Therefore, evaluations of porosity and permeability from XMCT images were limited to 0–10 cmbsf.

D. Porosity, Permeability, and Tortuosity From XMCT Images

The sediment physical properties of porosity, permeability, and tortuosity were all determined from 43 mm^3 XMCT images (Table III). Porosity determined from XMCT images displays a higher average value and a wider range of values than the conventional determinations made on cores (0.407 ± 0.0127 determined from images versus 0.367 ± 0.00433 determined with conventional measurements). Permeability values determined with a network model are roughly five times the values determined from CH permeameter evaluations, comparable to the values predicted using the KC equation, and ~45% higher than the EMT determinations. The sediment permeability was determined for two horizontal orientations (x and y) and one vertical orientation (z) using a network model to evaluate the volumetric XMCT images. Although permeability determinations are slightly less in the vertical orientation than in the horizontal orientations for the same volumes, the pressure applied in each direction was equal. Further evaluations on grain, such as the orientation of the major aspect ratio, and the pore paths through each plane, such as the direction and size of each pore path, need to be conducted to thoroughly address this result. Tortuosity, determined from volumetric XMCT images, had a mean value of 1.333 ± 0.00405. Tortuosity exhibited a narrow range, only 0.0145 over all locations and depths (0–10 cmbsf) at the

SAX04 site. The data presented in Table III suggest that surface sediment (0–10 cmbsf) samples at these five locations within the SAX04 site are nearly isotropic with respect to permeability and homogeneous with respect to porosity, permeability, and tortuosity. It is possible that this nearly isotropic characterization results from artifacts of image construction that rendered properties in the vertical axis slightly different than the same properties through the horizontal planes.

E. Grain-Contact Area and Coordination Number

The grain-segmentation process illustrated in Fig. 3 is automated, and provides a comprehensive set of parameters that characterize the grains and their packing structure. However, the automated algorithm is still being improved. Currently, it may break single grains into multiple parts, especially for the SAX04 sediment that comprises subangular grains of varied size with irregular geometries, which are far more difficult to construct from binary data than simple grains (e.g., spheres, cubes, cylinders) for which this algorithm is very accurate. Hence, for quantitative analysis, a manual refinement process is used to repair these discrepancies, before computing the grain parameters. The current manual refinement is time consuming (future versions will significantly improve the analysis and hopefully limit or negate this difficulty). Hence, only a single sample from the surface sediment (0–1 cmbsf), which was collected at the *R/V Seward Johnson* site, was evaluated for SAX04. This single sample provides a rare evaluation of grain contacts, grain coordination number, and grain-contact areas for well-sorted, angular, medium sand sediments [34]. In this sediment, the contact types are not limited to point contacts of ellipsoids, but range from point contacts to edge contacts to face contacts (Fig. 4). Additionally, the mean coordination number deviates from that of cubically packed spheres, which have a regular and constant coordination number of 6. The distribution of coordination numbers for SAX04 sands spans the coordination number determined from a hexagonal, close packing of spheres (i.e., 12). For this sample, the mean coordination number is 6.8 and the median coordination number is 6, but it should be kept in mind that the influence of these contacts on translation and rotation would be largely determined by surface contact area, which can be quantified, to the limits of the image resolution, from XMCT images (Fig. 5). Grain-contact areas are characterized as single point contacts where a single voxel from one grain contacts a voxel on another grain. Contacts that involve many voxels are characterized as large-area contacts (Fig. 6). Because calculations of contact and surface areas depend on voxel size, single point-contact areas are characterized as no smaller than the area of one voxel face (136 μm^2); smaller contacts are either below detection limits or assume this minimum surface area. This limitation on the minimum contact area arises because the pore space and the grain space are discretized in a binary fashion, as a 0 or a 1, respectively, based on the major constituent of the voxel volume. The resultant volume averaging that occurs within a voxel is therefore problematic when a single or small number of voxels are considered. Characterization of larger contact areas will prove more accurate, because there are more voxels per area and these broad-area contacts have contact areas that are $> 4000\ \mu m^2$ (Fig. 6).

V. Discussion

A. Porometric Properties

Laboratory determinations of porosity and permeability, made from sediments collected in diver cores, would seem comparable to determinations made using volumetric image analysis. Furthermore, lack of variability in values of porosity, density, and mean grain size in SAX04 cores suggests that the samples evaluated from XMCT images represent the sand sediments of the study area that was sampled and evaluated. Permeability determined using a CH permeameter and Darcy's law exhibits low variability: the CV for permeability in SAX04 sand is 18.3%, which is slightly less than the 21.1% determined for SAX99 and the 24.3% determined for North Sea sands [43]. Provided the high-resolution XMCT images and diver cores are representative of the *in situ* sand samples, we can assert that the sands that were sampled at the SAX04 experiment site are homogeneous from millimeter to centimeter scales. While it is tempting to extrapolate past the walls of the diver cores and into the surrounding region, heterogeneity due to shell deposits and in this case, mud, may have precluded the site from being fully homogeneous and isotropic through the acoustic paths, between the source and the receiver, over which sound speed and attenuation were determined.

Porosity determined by water-weight-loss measurements displays a narrower range of values than porosity determined from XMCT images (Tables I and III). This difference may be due to the averaging of small-scale fluctuations by the conventional method of measuring porosity (water weight loss) on larger, 2-cm-thick sediment volumes (54.7 cm^3), as opposed to the preservation of small-scale fluctuations within the small volumes (43 mm^3) imaged by XMCT. Porosity values determined from the smallest samples, the 2-D images, display the highest variability, which could indicate a correlation with sample size. This higher variability within porosity estimates from 2-D imagery suggests that a 9-mm^2 area may not fully represent the bulk properties within this geometrically complex sand. That is a representative elemental area for naturally occurring marine sands, with variability in grain size and geometrical shape typical of quartz, may be larger than the nine grain diameters that were suggested for uniform, laboratory-generated media or ellipsoidal sediments [27].

In comparison with previous work in medium-sized sand typical of this geographical area, conventionally determined values of porosity from cores are slightly lower (0.36 versus 0.37) at the SAX04 site than at the SAX99 site. The image-based determinations of porosity from SAX04 sediment in Table III (mean: 0.408) are also slightly less than those from the SAX99 sediment (mean: 0.414) [14]. This difference in permeability determinations is in keeping with previous work; image- and resistivity-based values of porosity were consistently higher than the water-weight-loss values determined from both the SAX99 and the SAX04 experiments [14], [15], [21], [33]. A methodological difference that may contribute to different results is that cores for image-based analysis were prepared almost immediately aboard ship and resistivity measurements were made *in situ* by inserting a resistivity probe into the sediments and predicting porosity using an empirical determination, called

Archie's law [35]. The conventional method of determining porosity in sands may consistently underestimate porosity due to water losses that occur during handling, transport to the laboratory, and subsequent analysis. A check on the magnitude of the loss of pore water during sectioning of the cores was made by comparing porosity determined from whole, unsectioned cores with that from cores sectioned at 2-cm intervals. Results indicate that SAX04 cores lost only 0.23% water during sectioning and previous checks indicated differences in water loss due to sectioning of less than 0.3%; in all cases, these samples were transported to the laboratory before analysis. Hence, settling of the sediment within the core tubes during transit to shore and before analysis may be the cause of the nearly 0.04 (10%) difference between porosity values determined from the conventional method and the XMCT imagery. Another possible source of this discrepancy are the potential errors associated with image data which result from fitting curvilinear surfaces to square pixels or cubic voxels during the segmentation process. The resulting problem is one of volume averaging, in which voxels that overlap grain and pore space are assigned intermediate gray-scale values, which may later be assigned to the pore phase even though nearly half of the space represented by the voxel comprises grain material. This problem is best addressed, and may be decreased, by using high-resolution images with as many voxels comprising the object as possible, although complex mathematical formulations are also sought [23]. If the resolution is insufficient to adequately define the pore-grain boundary in the XMCT images, resolution could contribute to the porosity variability and perhaps to discrepancies between image-based and conventional-based porosity values.

The range of tortuosity values is small for the 15 samples evaluated from the surficial 10 cm of sediment evaluated from several SAX04 study site locations (Table III). In all, five locations and three depths in the sediment were sampled from XMCT images. Mean tortuosity values are slightly lower than the mean values obtained from 2-D images for the SAX99 experiment (1.33 versus 1.49). However, the SAX04 determinations of tortuosity fall within the wider range of values from SAX99 (from 1.19 to 1.57) and are slightly lower than those predicted by Carman [1], [17]. The higher values of tortuosity obtained from 2-D images in SAX99 samples, as compared with 3-D images from SAX04, may be explained in the following way. In 2-D imagery, the pore path is restricted to a single plane, which may not be the shortest sinuous path from one pore body to another or through the sediment volume. In the 3-D images, tortuosity values are determined for independent paths, irrespective of orientation, and they exhibit little variation with depth or site location, therefore tortuosity is a reasonable indicator that SAX04 sediment samples are homogeneous with respect to pore path lengths within the top 10 cm of the seafloor sediment.

Variability in image-based determinations of permeability, as presented in Tables II and III, is probably a result of differences in pore radii and path lengths through the different sample planes. This type of path length variability typically occurs at different sample depths due to stratified sediments that have different grain sizes, shapes, and orientations that result in different sediment fabric and porosities with depth in the sediment. In terms of variability in grain sizes, such sands may be interbedded between fine-grained sediments, or there may be a wide range of grain size variations within specific sands. It may also be due to differences in grain alignment with preferential alignment along the major axis of grains; this is especially true with grains that have high aspect ratios, such as clays. In this case, aspect ratio, major to minor axis, was typically between 2 and 3. However, regarding the grain size distribution, the CV for mean grain size, bulk density, and porosity varied little throughout the SAX04 sediment [34]. Permeability of SAX04 sediment, whether determined from CH measurements or estimated from 2-D or 3-D image analysis, varies little within the specific analysis, which suggests that the differences in the mean values and the variability are related to the method of determination rather than to the sediment properties. Therefore, when determining the sediment properties and homogeneity, it is important to evaluate the range of values obtained by a single analysis and not the total range of values determined from all methods that were employed. The lowest permeability values were provided by core measurements using the CH method. The highest permeability values were provided by two different methods: the network modeling on XMCT images and the KC predictions; in both cases, a high value of 1.90×10^{-10} m^2 was obtained. The permeability predictions made using the KC equation typically fall between the CH measurements and the EMT modeling estimates of permeability. The KC predictions are two to three times higher than the measured permeability values, but in fairly good agreement with the permeability estimates from 2-D EMT and 3-D network modeling. However, the reason for the consistently lower measurements from the permeameter is unclear. Although consistently lower values may result from sediment compaction during handling or setup of the CH permeameter or during core collection, the potential for overestimates in permeability due to elevated fluid flow along the core tube walls remains possible. On the other hand, the image-based determinations may overestimate permeability by enlarging the pore volume and the pore throat sizes by including small grain features in the pore volume because these grain features are below the resolution limits of the XMCT. Hence, the pore space might be enlarged during segmentation, which would result in higher porosities and larger pore radii, thereby enhancing predictions of hydraulic conductivity and providing higher values of permeability. Because permeability correlates with porosity, it is not surprising that permeability is higher in the image analysis determinations than with traditional porosity determinations where the sample was scooped out of the core with a spoon. Permeability results from network modeling depend most significantly on the algorithm for computing pore-throat fluid conductances from the local pore sizes and shapes. The algorithm used here gives correct permeability values for packings of uniform-sized spheres and for computer generated packings. It is possible that this algorithm is less reliable for more angular grains and/or larger distributions of pore sizes due to an inability to account for the influence of small-scale grain roughness or surface morphology.

The evaluation of pore properties at different measurement scales is instructive toward determining sediment homogeneity with respect to these properties. The centimeter-scale analysis

of porosity from cores indicates that SAX04 sediment is homogeneous with respect to porosity and bulk density. The measurement of permeability in 13-cm cores, though more variable than porosity measurements, shows SAX04 sediment to be homogeneous at a scale of tens of centimeters within samples collected throughout the SAX04 study area. Porosity determined from volume XMCT images indicates low variability, if not homogeneity, at the millimeter-scale intervals from samples collected throughout the SAX04 site. The nearly uniform sediment tortuosity, as determined from XMCT images, indicates homogeneity at the pore scales to millimter scales in the upper 10 cm of the samples collected throughout the SAX04 site.

Evaluations of permeability in 3-D from the 3-D XMCT images using the network model may be used to evaluate variability in pore-scale flow through the sediment. That is, sediment isotropy or equality of flow in horizontal and vertical planes may be evaluated due to the unique ability of the network model to quantify flow through all sample planes. Regarding isotropy, as determined from equality in directional permeability, the results in Table III appear nonuniform because the vertical flow (z) was consistently lower than the horizontal flow (x and y). From the similar results for x and y orientations at sediment depths to 10 cm at the five locations within the SAX04 site, it appears that the sediment samples are isotropic to very slightly anisotropic. However, the difference in the network model determinations of permeability may be due to factors associated with image creation and analysis or due to compaction during core collection. Slight differences in permeability, such as these, may be significant in predictions of sound speed and attenuation, as was determined during SAX99 comparisons of acoustic measurements with model predictions [1]. Therefore, if the sediment is slightly anisotropic and the difference between vertical and horizontal permeability is real, uncertainty in sound-speed dispersion and attenuation determinations may result [1]. A second possibility is the following. If the sediment is slightly anisotropic at small scales, the isotropic assumption inherent to the Biot model might prove invalid in the sampled areas. However, the amount of variability required to be significant is unclear. Other factors that may yield discrepancies in high-frequency (>100 kHz) sound-speed and attenuation predictions made with the Biot model, such as intergranular motion, contact stress during loading of wet grains, or fluid acceleration between contacts during the passing of an acoustic wave, require further evaluation and novel experimentation [2], [3], [8], [44], [45].

B. Grain Contacts

Grain contacts can be evaluated directly within high-resolution, XMCT images of intact grain assemblages that are large enough (i.e., 6–10 grain diameters per dimension) to be considered representative of the bulk sediment [27]. Understanding grain contacts is important because they affect grain translation and rotation, which if present would result in a dynamic frame moduli. Such a situation would be a probable cause of sound-speed dispersion and attenuation within granular media at high acoustic frequencies (>100 kHz). Characterization of grain contacts is valuable in terms of determining their diversity and size distribution for implementation into discrete element, geotechnical, acoustic, or conceptual models [45]. The grain-contact data presented here indicate that intergranular interactions occur over small and large areas and that these areas may be highly variable for each grain. These contacts range from small-area point contacts or microasperities to edge and face contacts, which comprise large areas (Figs. 4 and 6). Consequently, the cumulative distribution of contact area per grain is far higher than is addressed by point-contact (Hertz–Mindlin) or microasperity-contact models. This may have important consequences regarding intergranular movement, or grain translation and rotation, which might be reduced during high-frequency insonification because the internal granular friction would be more difficult to overcome than with a point contact. However, if intergranular motion or grain translation and rotation were present, this would result in a dynamic frame modulus, sound-speed dispersion and acoustic attenuation [2], [3], [8]. While there is certainly a strong indication that granular contacts are often larger than a point, the actual size is difficult to quantify exactly, therefore the XMCT data may overestimate the contact area for several reasons. First, small-area contacts are restricted to the size of the voxel area; a direct artifact of the XMCT image is that the voxel has square sides, which are fitted to the grain's curvilinear surface features. These voxel faces may be larger or smaller than the actual contact. The XMCT images also lack the resolution to quantify small relief surface roughness, which would be necessary to quantify the coefficient of friction at each contact; in this case, scanning electron microscope (SEM) images could be used to determine the coefficient of friction. Coupling SEM with XMCT would help in modeling efforts to establish more realistic contact areas, coefficients of friction, and translation, rotation, or compression. In all, the large-area contacts with interlocking microasperities or surface areas are significantly different than the intergranular interactions addressed by classic contact models [22].

Although the number of contacts per grain (or grain coordination number) determined from the XMCT images falls within the theoretical range estimated for cubic-to-hexagonal close packing of monosized spherical particles (6 or 12 contacts per grain), the coordination number for some grains may be significantly higher. The primary difference with respect to coordination numbers is that SAX04 grains have a range of coordination numbers that spans that of the ideal packing of monosized spheres. Far more important to the understanding of frame softening or hardening and rotation or translation at the contacts is that many of the grains have contact areas that are much larger than can be addressed by commonly used contact models [2], [3], [22]. Because the contact areas are much larger, for the same number of contacts per grain, it seems that the force required to move grains would be significantly greater than would be predicted by point-contact models for spherical beads in ideal packings. This too would result in an overestimation of the potential for frame softening and grain motion in natural granular assemblages as compared with the potential for related processes to occur in spherical bead packs. Bench-scale acoustic experiments, coupled to XMCT

investigations that address a range of grain shapes with varied surface roughness, are required to address the importance of the grain surfaces on intergranular compression, rotation, and translation when a stress is applied, acoustic or otherwise [45].

VI. Summary

Porometric properties of sand cores from the SAX04 site display relatively small variations in values obtained from several independent techniques. Due to this small degree of variability, the sampled sediment appears homogeneous in the top 10 cm at the five locations sampled for these analyses. This homogeneity is apparent from the submillimeter pore scale to tens of centimeters at the core scale at each of the sampled locations, suggesting that the porometric parameters employed by high-frequency acoustic models are appropriate throughout the SAX04 site within these sand sediments. The influence of mud that may have been present between acoustic transducers was not addressed here.

Sediment porosity values displayed a narrow range, from 0.367 to 0.369, when determined by water weight loss on 54 cm^3 sized samples, but ranged more widely, from 0.385 to 0.436, when determined from 2-D images, which were 9 mm^2. The porosity values obtained from 2-D image analysis remain comparable to those determined by 3-D image analysis, but display a higher mean value and greater variability (0.414 ± 0.0322 and 0.408 ± 0.0122, for 2-D and 3-D imagery, respectively). This result may occur because 2-D image porosity determinations evaluate a single horizontal slice of the XMCT volume, whereas porosity determination from 3-D images evaluates 300 slices of the same xy dimension. Sediment permeability ranges from 2.8×10^{-11} m^2 to 19.0×10^{-11} m^2 depending on the methodology used. Within method variability is much smaller. The mean value of permeability measured from cores is 3.11×10^{-11} m^2; the mean value predicted from the KC equation is 1.45×10^{-10} m^2; the mean value estimated by EMT from 2-D imagery is 8.35×10^{-11} m^2; and the mean value estimated by network modeling from 3-D imagery is 1.38×10^{-10} m^2. These permeability values are typical for coastal sand sediments. Sediment tortuosity was determined from XMCT images to range from 1.332 to 1.337. This low amount of variability indicates that the sediment is homogeneous throughout the evaluated sediments. Network model comparisons indicate that the sediment may be slightly anisotropic when comparisons between vertical and horizontal permeability are made. These comparisons were limited to XMCT data obtained using a network model.

Grain-contact areas range in size and depend upon the complexity of the surface geometry. Because natural grains are composed of many surfaces with elevated points, imaged contact areas are often small (1–4 voxels), and not entirely consistent in this respect with point-contact models, such as that developed by Walton [22]. Additionally, numerous grain contacts have areas that are much greater than the area occupied by a point contact, therefore a significant number of contacts deviate from what is described and modeled with point contacts [2], [3], [8]. Based on these data, it appears that point-contact models have a limited, but often very useful, applicability to studies of natural sediments and in descriptions of sedimentary processes. Our continued pursuit will be to evaluate granular interactions to determine contact shape, size, frequency, and response to stresses that impart intergranular shear, translation, and rotation during insonification [45].

Acknowledgment

The authors would like to thank K. Wilson for assisting with 2-D data sets and providing images of core heterogeneity. E. Braithwaite wrote "grainspinner" which was instrumental in enabling individual grains to be visualized easily. The NRL dive team of W. C. Vaughan, M. Richardson, K. Briggs, and R. Ray collected the core samples with the assistance of the crews of the *R/V Seward Johnson* and *R/V Pelican*.

References

[1] K. L. Williams, D. R. Jackson, E. I. Thorsos, D. Tang, and S. G. Schock, "Comparison of sound speed and attenuation measured in a sandy sediment to predictions based on the Biot theory of porous media," *IEEE J. Ocean. Eng.*, vol. 27, no. 3, pp. 413–428, Jul. 2002.

[2] M. J. Buckingham, "Wave propagation, stress relaxation, and grain-to-grain shearing in saturated, unconsolidated marine sediments," *J. Acoust. Soc. Amer.*, vol. 108, no. 6, pp. 2796–2815, 2000.

[3] B. T. Hefner and K. L. Williams, "Sound speed and attenuation measurements in unconsolidated glass-bead sediments saturated with viscous pore fluids," *J. Acoust. Soc. Amer.*, vol. 120, no. 5, pp. 2538–2549, 2006.

[4] E. I. Thorsos, SAX04 Summary, [Online]. Available: http://www.apl.washington.edu/projects/SAX04/summary.html

[5] B. J. Kraft and C. de Moustier, "Detailed bathymetric surveys offshore Santa Rosa Island, FL: before and after Hurricane Ivan (September 16, 2004)," *IEEE J. Ocean. Eng.*, vol. 35, no. 3, pp. 453–470, Jul. 2010.

[6] M. A. Biot, "Theory of propagation of elastic waves in a fluid saturated porous solid. II. Higher frequency range," *J. Acoust. Soc. Amer.*, vol. 28, no. 2, pp. 179–189, 1956.

[7] R. D. Stoll, "Sediment acoustics," in *Lecture Notes in Earth Sciences*, S. Bhattacharji, G. M. Friedman, H. J. Neugenbauer, and A. Seilacher, Eds. New York: Springer-Verlag, 1989, vol. 26, p. 16.

[8] N. P. Chotiros and M. J. Isakson, "Acoustic virtual mass of granular media," *JASA Express Lett.*, vol. 121, no. 2, pp. EL70–EL76, 2007.

[9] M. A. Biot, "Generalized theory of acoustic propagation in porous dissipative media," *J. Acoust. Soc. Amer.*, vol. 34, pp. 1254–1264, 1962.

[10] K. L. Williams, "An effective density fluid model for acoustic propagation in sediments derived from Biot theory," *J. Acoust. Soc. Amer.*, vol. 110, no. 5, pp. 2276–2281, 2001.

[11] P. S. Wilson, A. H. Reed, J. C. Wilbur, and R. A. Roy, "Evidence of dispersion in an artificial water-saturated sand sediment," *J. Acoust. Soc. Amer.*, vol. 121, no. 2, pp. 824–832, 2007.

[12] M. A. Zimmer, M. Prasad, G. Mavko, and A. Nur, "Seismic velocities of unconsolidated sands: Part 1—Pressure trends from 0.1 to 20 MPa," *Geophysics*, vol. 72, no. 1, pp. E1–E13, 2007.

[13] R. Ehrlich, S. Kennedy, S. J. Crabtree, and R. L. Cannon, "Petrographic image analysis, I, analysis of reservoir pore complexes," *J. Sediment. Petrol.*, vol. 54, no. 4, pp. 1365–1378, 1984.

[14] A. H. Reed, K. B. Briggs, and D. L. Lavoie, "Porometric properties of siliciclastic marine sand: A comparison of traditional laboratory measurements with image analysis and effective medium modeling," *IEEE J. Ocean. Eng.*, vol. 26, no. 1, pp. 4–25, Jan. 2002.

[15] C. W. Curry, R. H. Bennett, M. H. Hulbert, K. J. Curry, and R. W. Faas, "Comparative study of sand porosity and a technique for determining porosity of undisturbed marine sediment," *Mar. Georesources Geotechnol.*, vol. 22, no. 4, pp. 231–252, 2004.

[16] F. A. L. Dullien, *Porous Media: Fluid Transport and Pore Structure*, 2nd ed. New York: Academic, 1992, pp. 9–11.

[17] P. Carman, *Flow of Gases Through Porous Media*. New York: Academic, 1956, pp. 13, 45–47.

[18] J. Koplik, C. Lin, and M. Vermette, "Conductivity and permeability from microgeometry," *J. Appl. Phys.*, vol. 56, no. 11, pp. 3127–3131, 1984.

[19] K. E. Thompson and H. S. Fogler, "Modeling flow in disordered packed beds from pore-scale fluid mechanics," *AIChe J.*, vol. 43, no. 6, pp. 1377–1389, 1997.
[20] M. B. Clennell, "Tortuosity: A guide through the maze," in *Developments in Petrophysics*, M. A. Lovell and P. K. Harvey, Eds. Bath, U.K.: , 1997, pp. 299–344, Geological Society Special Publication no. 122.
[21] K. J. Curry, M. Abril, J. B. Avril, C. W. Curry, R. H. Bennett, and M. H. Hulbert, "A technique for processing undisturbed marine sand sediments and reconstructing fabric and porometry," *J. Sed. Res.*, vol. 72, no. 6, pp. 933–937, 2002.
[22] K. Walton, "The effective elastic moduli of a random packing of spheres," *J. Mech. Phys. Solids*, vol. 35, pp. 213–226, 1987.
[23] K. E. Thompson, C. S. Willson, and W. L. Zhang, "Quantitative computer reconstruction of particulate materials from microtomography images," *Powder Technol.*, vol. 163, no. 3, pp. 169–182, 2006.
[24] W. Zhang, K. E. Thompson, A. H. Reed, and L. Beenken, "Relationship between packing structure and porosity in fixed beds of equilateral cylindrical particles," *Chem. Eng. Sci.*, vol. 61, no. 24, pp. 8060–8074, 2006.
[25] P. Cheng and C. T. Hsu, "The effective stagnant thermal conductivity of porous media with periodic structures," *J. Porous Media*, vol. 2, no. 1, pp. 19–38, 1999.
[26] J. T. Fredrich, B. Menendez, and T. F. Wong, "Imaging the pore structure of geomaterials," *Science*, vol. 268, no. 5208, pp. 276–279, 1995.
[27] R. I. Al-Raoush and C. S. Willson, "Extraction of physically realistic pore network properties from three-dimensional synchrotron X-ray microtomography images of unconsolidated porous media systems," *J. Hydrology*, vol. 300, pp. 44–64, 2005.
[28] P. M. Doyen, "Permeability, conductivity, and pore geometry of sandstone," *J. Geophys. Res.*, vol. 93, no. B7, pp. 7729–7740, 1988.
[29] K. E. Thompson, C. S. Willson, C. D. White, S. Nyman, J. Bhattacharya, and A. H. Reed, "Application of a new grain-based reconstruction algorithm to microtomography images for quantitative characterization and flow modeling," presented at the Annu. Tech. Conf. Exhibit., Dallas, TX, Oct. 9–12, 2005, SPE 95887.
[30] L. J. Doyle and T. N. Sparks, "Sediments of the Mississippi, Alabama and Florida (MAFLA) continental shelf," *J. Sediment. Petrol.*, vol. 50, no. 3, pp. 905–915, 1980.
[31] M. D. Richardson, K. B. Briggs, D. L. Bibee, P. A. Jumars, W. B. Sawyer, D. B. Albert, R. H. Bennett, T. K. Berger, M. J. Buckingham, N. P. Chotiros, P. H. Dahl, N. T. Dewitt, P. Fleischer, R. Flood, C. F. Greenlaw, D. V. Holliday, M. H. Hulbert, M. P. Hutnak, P. D. Jackson, J. S. Jaffe, H. P. Johnson, D. L. Lavoie, A. P. Lyons, C. S. Martens, D. E. McGhee, K. D. Moore, T. H. Orsi, J. N. Piper, R. I. Ray, A. H. Reed, R. F. L. Self, J. L. Schmidt, S. G. Schock, F. Simonet, R. D. Stoll, D. Tang, D. E. Thistle, E. I. Thorsos, D. J. Walter, and R. A. Wheatcroft, "An overview of SAX99: Environmental considerations," *IEEE J. Ocean. Eng.*, vol. 26, no. 1, pp. 26–53, Jan. 2001.
[32] Sediment Acoustic Experiment—2004 (SAX04), Sep. 8, 2007 [Online]. Available: http://www.apl.washington.edu/projects/SAX04/chirp.html
[33] D. Tang, K. B. Briggs, K. L. Williams, D. R. Jackson, and E. I. Thorsos, "Fine-scale volume heterogeneity measurements in sand," *IEEE J. Ocean. Eng.*, vol. 27, no. 3, pp. 546–560, Jul. 2002.
[34] W. C. Vaughan, K. B. Briggs, J. W. Kim, T. S. Bianchi, and R.W. Smith, "Storm-generated sediment distribution along the northwest Florida inner continental shelf," *IEEE J. Ocean. Eng.*, vol. 34, no. 4, pp. 495–515, Oct. 2009.
[35] K. B. Briggs, A. H. Reed, D. R. Jackson, and D. Tang, "Fine-scale volume heterogeneity in a mixed sand/mud sediment off Fort Walton Beach, FL," *IEEE J. Ocean. Eng.*, vol. 35, no. 3, pp. 471–487, Jul. 2010.
[36] R. M. McMullen and J. R. L. Allen, "Preservation of sedimentary structures in wet unconsolidated sands using polyester casting resins," *Mar. Geol.*, vol. 1, no. 1, pp. 88–97, 1964.
[37] K. E. Thompson, "Computing particle surface areas and contact areas from three-dimensional tomography data of particulate materials," *Part. Part. Syst. Charact.*, vol. 24, pp. 440–452, 2007.
[38] J. M. Hovem and G. D. Ingram, "Viscous attenuation of sound in saturated sand," *J. Acoust. Soc. Amer.*, vol. 66, no. 6, pp. 1807–1812, 1979.
[39] B. P. Flannery, H. W. Deckman, W. G. Roberge, and K. L. D'Amico, "Three-dimensional x-ray microtomography," *Science*, vol. 237, no. 4821, pp. 1439–1444, 1987.
[40] W. Oh and B. Lindquist, "Image thresholding by indicator kriging," *IEEE Trans. Pattern Anal. Mach. Intell.*, vol. 21, no. 7, pp. 590–602, Jul. 1999.
[41] W. B. Lindquist and A. Venkatarangan, "Investigating 3D geometry of porous media from high resolution images," *Phys. Chem. Earth A–Solid Earth Geodesy*, vol. 24, no. 7, pp. 593–599, 1999.
[42] S. L. Bryant, D. W. Mellor, and C. A. Cade, "Physically representative network models of transport in porous-media," *AIChE J.*, vol. 39, no. 3, pp. 387–396, 1993.
[43] J. Lindblad, "Surface area estimation of digitized 3D objects using weighted local configurations," *Image Vis. Comput.*, vol. 23, pp. 111–122, 2005.
[44] D. R. Jackson and M. D. Richardson, *High-Frequency Seafloor Acoustics*. New York: Springer-Verlag, 2007, p. 95.
[45] D. M. Cole and J. F. Peters, "A physically based approach to granular media mechanics: Grain-scale experiments, initial results and implications to numerical modeling," *Granular Matter*, vol. 9, pp. 309–321, 2007.

Allen H. Reed received the B.S. degree in oceanography from Humboldt State University, Arcata, CA, in 1996, the M.S. degree in marine science from The University of Southern Mississippi, Hattiesburg, in 1999, and the Ph.D. degree in coastal studies from the Louisiana State University, Baton Rouge, in 2004.

Currently, he is a Geologist focusing on marine sedimentology in the littoral and oceanic environments. His primary interest is in determining sediment physical properties, sediment fluid and thermal conductivities, and geotechnical properties. He has worked in the Seafloor Sciences Branch at the Naval Research Laboratory, Naval Space Center, MS, for 12 years. He has worked in the Baltic, the Beaufort Sea, off the coast of Brazil and in several coastal environments surrounding the continental United States.

Karsten E. Thompson received the Ph.D. degree in chemical engineering from University of Michigan, Ann Arbor, in 1996.

Currently, he is a Professor at the Department of Chemical Engineering, Louisiana State University, Baton Rouge. His research focus is on transport and reaction in porous media, low-Reynolds number flow and mass transfer, and computational methods.

Kevin B. Briggs received the B.S. degree in biology from Florida Atlantic University, Boca Raton, in 1975, the M.S. degree in zoology from the University of Georgia, Athens, in 1978, and the Ph.D. degree in marine geology and geophysics from the Rosenstiel School of Marine and Atmospheric Science, University of Miami, Miami, FL, in 1994.

He began working at the Naval Ocean Research and Development Activity, now part of the Naval Research Laboratory (NRL), at the Stennis Space Center, MS, in 1979, where he was involved in research on the effects of environmental processes on sediment geoacoustic properties. He has participated in many shallow-water high-frequency acoustics experiments as an investigator of geoacoustic and roughness properties of the seafloor. He is currently engaged in research on characterization of sediment interface roughness and volume heterogeneity for high-frequency acoustic modeling. He has over 40 published articles on physical and acoustic properties of the seafloor.

Dr. Briggs is a member of the Acoustical Society of America, the American Geophysical Union, and Sigma Xi.

Clinton S. Willson received the B.S. degree in aerospace engineering from Pennsylvania State University, University Park, in 1985 and the M.S. degree in environmental health engineering and the Ph.D. degree in civil engineering from the University of Texas at Austin, in 1994 and 1997, respectively.

Currently, he is an Associate Professor at the University Department of Civil and Environmental Engineering, Louisiana State University, Baton Rouge. His research focus is in the area of environmental fluid mechanics with projects ranging from pore-scale imaging of single-phase and multiphase porous media systems to physical and numerical modeling of the hydrodynamics and sediment transport of the lower Mississippi River.